Gap opening and tuning in single-layer graphene with combined electric and magnetic field modulation*

Lin Xin(林 鑫), Wang Hai-Long(王海龙), Pan Hui(潘 晖), and Xu Huai-Zhe(许怀哲)†

Department of Physics, Beihang University, Beijing 100191, *China*

(Received 9 December 2010; revised manuscript received 8 January 2011)

The energy band structure of single-layer graphene under one-dimensional electric and magnetic field modulation is theoretically investigated. The criterion for bandgap opening at the Dirac point is analytically derived with a two-fold degeneracy second-order perturbation method. It is shown that a direct or an indirect bandgap semiconductor could be realized in a single-layer graphene under some specific configurations of the electric and magnetic field arrangement. Due to the bandgap generated in the single-layer graphene, the Klein tunneling observed in pristine graphene is completely suppressed.

Keywords: gap opening at Dirac point, single-layer graphene, electric and magnetic superlattice, second-order perturbation

PACS: 73.43.Cd, 73.61.Wp, 73.50.Bk **DOI:** 10.1088/1674-1056/20/4/047302

1. Introduction

Graphene has been the subject of intensive experimental and theoretical studies since it was experimentally realized by Novoselov *et al.* in 2004.[1] The high mobility of electrons in graphene at room temperature[2,3] makes it one of the most promising candidates for the next generation of nanoelectronics. Graphene is a structure in which a single-layer carbon atoms are arranged in honeycomb lattice structure with two atoms per primitive cell.[4] The Fermi-energy ($E_{\rm F}$) of pristine grapheme is located at the so-called Dirac points[5] (K and K'), which are the high-symmetry points of the hexagonal Brillouin zone (BZ). The low energy excitation around the Dirac points is normally described by a massless Dirac-like Hamiltonian.[6,7] Graphene exhibits many unusual properties,[6−10] such as Klein tunneling, an unconventional integer quantum Hall effect and minimum conductivity, etc. It is well known that pristine graphene is a zero-gap semimetal, and it always has zero energy finite conductivity, which prevents pinch off of the field effect transistor, so pristine graphene can not provide an on–off signal ratio,[1,10,11] an essential feature of traditional semiconductors. Thus, the opening and tuning bandgap of graphene are especially crucial to the practical application of graphene to electronic devices.

Recently, several schemes have been proposed to open and tune the bandgap of graphene, such as graphene-substrate interaction,[12] patterned hydrogen adsorption,[13] controlled adatom deposition,[14,15] physical cutting single-layer graphene into nanoribbons[16−18] or etching it into antidot lattices.[19] However, the existence of a substrate-induced gap for graphene deposited on SiC is still under debate.[20,21] It is difficult to control the gap width of graphene nanoribbons as it is very sensitive to width and edge geometry of nanoribbons, as well as to chemical functionalization. Furthermore, the present technology cannot widely achieve the pattern hydrogen adsorption or the construction of antidot lattices.

Depositing patterned gates and/or ferromagnetic stripes on the surface of semiconductor heterostructures has been widely used to modulate transport behaviours in two-dimensional electron gases (2DEGs).[22−26] This technique could also be applied to graphene[27,28] once the graphene sheet is covered by an insulating layer, and has recently been demonstrated feasible.[29−32] Recently, Park *et al.*[33−35] theoretically analysed the band structure of single-layer graphene modulated by one-dimensional (1D) or two-dimensional (2D) electrical superlattices (ESs). Some interesting electronic properties have been revealed, such as the anisotropic renormalization of group ve-

*Project supported by the National Natural Science Foundation of China (Grant Nos. 60776067 and 10974011).

†Corresponding author. E-mail: hzxu@buaa.edu.cn

© 2011 Chinese Physical Society and IOP Publishing Ltd

locity for low energy charge carriers;[33−35] the generation of extra Dirac points when the applied gate voltage is beyond a threshold;[33−37] the unusual properties of Landau levels and the quantum Hall effect for these extra Dirac fermions.[38] It is found that a bandgap could be opened only at the boundary of the ES BZ,[33−35] while the gapless band structure at the Dirac point is always remained for 1D ESs.[33−42] In addition, the band structure of single-layer graphene under a magnetic superlattice (MS) has been extensively studied,[43−48] and it is confirmed that a MS is also insufficient to open a bandgap at the original Dirac point in single-layer graphene.

In this paper, we will systemically analyse the modulation effect of a combined 1D electric and magnetic field on the graphene energy spectrum with an emphasis on how to generate and tune a bandgap at the Dirac point. We will derive a criterion for bandgap opening at the Dirac point using a two-fold degeneracy second-order perturbation method. It is shown that a bandgap cannot be opened at the Dirac point using an electric or a magnetic field. However, a bandgap can be generated when the modulating electric and magnetic fields are arranged in some specific spatial configurations. Single-layer graphene can be a direct or an indirect bandgap semiconductor, depending on the electric and the magnetic field spatial configurations. It is also shown that the band top/bottom positions and the gap width can be tuned continuously by varying the electric and/or magnetic field in strength. The transport properties of single-layer graphene with finite periods of electric and magnetic field modulations clearly show that Klein tunneling in the low energy region in pristine graphene is completely suppressed due to the bandgap opening. The combined electric and magnetic field modulation provides a new way to control the bandgap of graphene, which is believed to be quite useful for realizing graphene-based devices.

The rest of the present paper is organized as follows. In Section 2 we introduce the two-fold degeneracy second-order perturbation and analytically derive the criterion for gap opening at the Dirac point by this method. In Section 3, we give several examples to show that single-layer graphene can become a direct or an indirect bandgap semiconductor depending on the spatial arrangements of the electric and magnetic field, and we also analyse the transport property of graphene under finite periods of electric and magnetic field modulation. In Section 4, we summarize our results and draw conclusions.

2. Theoretical analysis

Assuming that the spatial period of the external potential is much larger than the graphene lattice constant ($\sim$ 1.42 Å, 1 Å=0.1 nm),[4] the intervalley scattering can be neglected. In a long-wavelength approximation, the Dirac-like Hamiltonian around the K point is expressed as (with $\hbar = c = 1$)

$$H = v_{\mathrm{F}}\left(-\mathrm{i}\nabla + e\boldsymbol{A}\right)\cdot\boldsymbol{\sigma} + e\boldsymbol{U}\cdot\boldsymbol{I}, \tag{1}$$

where $v_{\mathrm{F}} = 10^6$ m/s is the Fermi velocity, e is the absolute value of the electron charge, $\boldsymbol{A}$ is the vector potential, $\boldsymbol{\sigma} = (\sigma_x, \sigma_y)$ is a 2×2 Pauli matrix vector and $\boldsymbol{I}$ is the 2×2 unit matrix.

We choose the Landau gauge as $A(x) = \left(0,\ \int B(x)\,\mathrm{d}x,\ 0\right)$, and the Dirac-like Hamiltonian is rewritten as

$$H = H_0 + H' \tag{2a}$$

with

$$H_0 = v_{\mathrm{F}}\begin{pmatrix} 0 & \hat{k}_x - \mathrm{i}\,\hat{k}_y \\ \hat{k}_x + \mathrm{i}\,\hat{k}_y & 0 \end{pmatrix}, \tag{2b}$$

$$H' = \begin{pmatrix} -eU & -\mathrm{i}\,ev_{\mathrm{F}}A \\ \mathrm{i}\,ev_{\mathrm{F}}A & -eU \end{pmatrix}. \tag{2c}$$

Here, H' is treated as the perturbation induced by the weak external potentials.

In the following, the two-fold degeneracy second-order perturbation is used at the Dirac point. For simplicity we further assume that $\langle B(x)\rangle = 0$, $\langle U(x)\rangle = 0$ and $\langle A(x)\rangle = 0$, so the first-order perturbation is zero. We need to consider the second-order perturbation. The secular equation of the second-order perturbation at the Dirac point is obtained as

$$\begin{pmatrix} H_{11} & H_{12} \\ H_{21} & H_{22} \end{pmatrix}\psi - E * I\psi = 0, \tag{3}$$

with

$$H_{ij} = \sum_{s,k}\frac{\langle\psi_i|H'|\psi^0_{s,k}\rangle\langle\psi^0_{s,k}|H'|\psi_j\rangle}{0 - E}, \tag{4}$$

where $\psi^0_{s,k}$ is the eigenstate of H_0, and ψ_i is the zero-order wavefunction ($i = 1, 2$) at Dirac point of two-fold degeneracy. The box normalization wavefunctions are given as

$$\psi^0_{s,k}(x,y) = \frac{1}{\sqrt{L}}\cdot\frac{1}{\sqrt{2}}\begin{pmatrix} 1 \\ s.\mathrm{e}^{\mathrm{i}\,\theta_k} \end{pmatrix}\mathrm{e}^{\mathrm{i}\,k_x x}.\mathrm{e}^{\mathrm{i}\,k_y y}, \tag{5}$$

$$\psi_1 = \frac{1}{\sqrt{L}}\begin{pmatrix}1\\0\end{pmatrix}, \quad \psi_2 = \frac{1}{\sqrt{L}}\begin{pmatrix}0\\1\end{pmatrix}, \tag{6}$$

where $s = \pm 1$ is the band index, $1/\sqrt{L}$ is a box normalization factor, $\boldsymbol{k} = (k_x,\ k_y)$ is the wave vector of the plane wavefunction, and θ_k is the polar angle of the wave vector $\boldsymbol{k}$.

Inserting both Eq. (5) and Eq. (6) into Eq. (4), the matrix elements of the secular equation are derived as (see Appendix)

$$H_{12} = H_{21} = 0, \tag{7}$$

$$H_{11} = -H_{22} = \int\limits_{s=1,k_x>0,k_y>0.} \mathrm{d}E k \mathrm{d}\theta_k \rho\left(E,\theta_k\right) I_{11}, \tag{8}$$

where

$$\begin{aligned} I_{11} =& \frac{1}{L^2}\frac{1}{E} 8 v_{\mathrm{F}} \cos\theta_k \Big(\int_0^L \mathrm{d}x e U\left(x\right) \sin\left(k_x x\right) \\ & \times \int_0^L \mathrm{d}x e A\left(x\right) \cos\left(k_x x\right) \\ & - \int_0^L \mathrm{d}x e U\left(x\right) \cos\left(k_x x\right) \\ & \times \int_0^L \mathrm{d}x e A\left(x\right) \sin\left(k_x x\right) \Big). \end{aligned} \tag{9}$$

The eigenvalues of the secular equation can be easily obtained from Eq. (3) as

$$E = \pm H_{11}. \tag{10}$$

It is explicit that when $H_{11} \neq 0$, the two-fold degeneracy at the Dirac point is broken and a bandgap is generated at the Dirac point. Thus, equation (8) can be considered as a criterion for gap opening at the Dirac point. It is noticed that H_{11} can be regarded as a mass term of Dirac fermions.[49] This mass is different from that induced by the on-site potential by patterned substrate.[8] As the two species of Dirac points are described by the same Dirac-like Hamiltonian, the gap will be generated at both valleys.

Using Eq. (8) we have investigated the gap opening possibilities in several model structures reported in previous literature.

Case 1 The 1D square ES (Refs. [33]–[35], [37], [41] and [42]). $H_{11} = 0$, there is no bandgap at the original Dirac point. While extra Dirac points will emerge in the $k_x = 0$ direction when electric potential beyond a threshold of $U_0 = 4\pi\hbar v_{\mathrm{F}}/L$, and bandgap can be generated at these extra Dirac points in some special electric potential forms.[42]

Case 2 The 1D δ-function ES (Ref. [39]). Again we have $H_{11} = 0$, there is not a bandgap at the original Dirac point. The Dirac point will become a Dirac line when $P = (n + 1/2)\pi\hbar v_{\mathrm{F}}/L$.[39]

Although we have obtained Eq. (8) under the assumption of $\langle U(x)\rangle = 0$, it can be easily extended to $\langle U(x)\rangle \neq 0$, as $U(x)$ can be divided into two parts, i.e., $U(x) = U_1(x)+U_2(x)$ with $\langle U_1(x)\rangle = 0$ and $U_2(x)$ a constant. The constant $U_2(x)$ will shift the whole band structure upward or downward, which does not change the criterion for gap opening at the Dirac point when $\langle U(x)\rangle \neq 0$.

Case 3 The 1D MS $\langle B(x)\rangle = 0$ (Refs. [43], [45], [46] and [48]). In this case, $H_{11} = 0$. The bandgap cannot be generated at the Dirac point. Although the MS will destroy the time reversal symmetry of the system, it cannot raise or reduce the eigenenergy of the two-fold zero energy states. For the MS $\langle B(x)\rangle \neq 0$ case, we can also choose an appropriate gauge to make $\langle A(x)\rangle = 0$ by plus or minus a constant, then we can still have $H_{11} = 0$. This can be seen from the reported results, and the band structure will be quantized into Landau levels, but the zero-energy state is always present in such an MS.[44,48]

Case 4 The 1D ES+MS in which $\langle U(x)\rangle = 0$ and $\langle B(x)\rangle = 0$ (Refs. [49] and [50]). For the spatial arrangement of electric and magnetic potentials described by the second example of Refs. [49] and [50], we have $H_{11} \neq 0$, and a bandgap will be generated at the Dirac point, which accords well with the results in Refs. [49] and [50].

It is worthwhile pointing out that in our derivation of the two-fold second-order perturbation, $U(x)$ and $B(x)$ or $A(x)$ are not required to have a spatial periodicity. In fact, $U(x)$ and $A(x)$ can be in arbitrary forms of functions. From Eq. (9), H_{11} is a function of the coupling between electric field and magnetic field. Whenever $U(x) = 0$ or $A(x) = 0$, $H_{11} = 0$, which means that the single-layer graphene will always be gapless at the Dirac point with electric field or magnetic field separately. A gap can be generated only under the modulation of combined the electric and the magnetic fields. As both $\sin(k_x x)$ and $\cos(k_x x)$ are simultaneously present in the integration of Eq. (9), $H_{11} \neq 0$ happens only when the electric and the magnetic fields are arranged in some specific spatial configurations. Because $\sin(k_x x)$ is an odd function and $\cos(k_x x)$ an even function, it is easy to deduce that $H_{11} \neq 0$ for $U(x) = U(-x)$ and $A(x) = -A(-x)$, or, $U(x) = -U(-x)$ and $A(x) = A(-x)$, as shown

in Fig. 1(b) and in Refs. [49] and [50]. But for the structure illustrated in Fig. 1(c), where $U(x) = U(-x)$ and $A(x) = A(-x)$, or, $U(x) = -U(-x)$ and $A(x) = -A(-x)$, we will have $H_{11} = 0$, thus it cannot generate a bandgap at the Dirac point.

3. Numerical results

To understand the spatial arrangement effect of the electric and magnetic fields on the gap opening at the Dirac point of single-layer graphene, we numerically calculate the band structure of several models. To simplify the calculation, we assume that the electric and the magnetic fields are periodically arranged in the x direction.

Firstly, we assume that both the electric and the magnetic potential are arranged in anti-symmetry as shown schematically in Fig. 1(b).[1)] The magnetic field and the electrostatic potential are taken as

$$\begin{aligned} B =& \hat{z} \cdot B \sum_{n\in Z} \left(\delta\left(x - \left(n - \frac{1}{4}\right) L_0\right) - \delta\left(x - \left(n - \frac{2}{4}\right) L_0\right) + \delta\left(x - \left(n - \frac{3}{4}\right) L_0\right) - \delta\left(x - (n-1)\, L_0\right) \right), \\ U =& - U \sum_{n\in Z} \left(\Theta\left(x - nL_0\right) - \Theta\left(x - \left(n - \frac{1}{4}\right) L_0\right) + \Theta\left(x - \left(n - \frac{2}{4}\right) L_0\right) - \Theta\left(x - \left(n - \frac{3}{4}\right) L_0\right) \right), \end{aligned} \tag{11}$$

where Θ is a step function. This structure can be realized experimentally by using periodically patterned gates and magnetic stripes on the surface of single-layer graphene.[27,28,51]

The energy dispersion relation is obtained by using the transfer matrix method in Kroning–Penney model as

$$\cos(\kappa_x l) = \frac{1}{2} \operatorname{Tr}(S_{U+} S_{A+} S_{U-} S_{A-}), \tag{12}$$

in which

$$S_{U\pm} = \begin{pmatrix} \cos(k_{xU\pm} b) - k_y / k_{xU\pm} \sin(k_{xU\pm} b) & -\mathrm{i}(E \mp U / k_{xU\pm}) \sin(k_{xU\pm} b) \\ -\mathrm{i}(E \mp U / k_{xU\pm}) \sin(k_{xU\pm} b) & \cos(k_{xU\pm} b) + k_y / k_{xU\pm} \sin(k_{xU\pm} b) \end{pmatrix}, \tag{13a}$$

and

$$S_{A\pm} = \begin{pmatrix} \cos(k_{xA\pm} w) - (k_y \pm A / k_{xP\pm}) \sin(k_{xA\pm} w) & -\mathrm{i}(E / k_{xA\pm}) \sin(k_{xA\pm} w) \\ -\mathrm{i}(E / k_{xA\pm}) \cdot \sin(k_{xA\pm} w) & \cos(k_{xA\pm} w) + (k_y \pm A / k_{xA\pm}) \sin(k_{xA\pm} w) \end{pmatrix}. \tag{13b}$$

Here, we have used the dimensionless units as: $l \to l_0 l$, $k \to k_0 k$, $E \to E_0 E$, and $A \to B_0 l_0 A$, where $k_0 = 1/l_0$, $E_0 = \hbar v_{\mathrm{F}} / l_0$, and $B_0 = \hbar / e l_0^2$.

In Fig. 1(b), there are two central symmetry points S_1 and S_2. At point S_1, $U(x) = U(-x)$ and $A(x) = -A(-x)$; while at point S_2, $U(x) = -U(-x)$ and $A(x) = A(-x)$, thus a bandgap will be generated at Dirac point. It can be demonstrated that the system Hamiltonian H_1 for the model 1 satisfies,

$$(SP) H_1 (SP)^{-1} = -H_1, \tag{14a}$$

$$S H_1 S^{-1} = H_1', \tag{14b}$$

where $S = \begin{pmatrix} 0 & 1 \\ -1 & 0 \end{pmatrix} \cdot c$ is the single valley time reversal operator, with c being the operator of complex conjugation; P is the parity operator; $H_1'(x)$ describes the structure of $H_1(x)$ in opposite order; $H_1'(x) = H_1(-x)$ means that the band structures described separately by $H_1'(x)$ and $H_1(-x)$ are identical with each other, thus, $E_1(s,\ k_y) = E_1(s,\ -k_y)$, the band structure has a mirror symmetry with respect to $k_y = 0$ plane. The operator SP in Eq. (14a) translates the electron-like state into a hole-like state, leading to $E_1(s, k_y) = -E_1(-s, k_y)$, the electron band and hole band are mirror symmetry with respect to $E = 0$ plane. The single-layer graphene is a direct bandgap semiconductor. We will only give the electron band of model 1 in the following discussion for simplicity.

[1)] UC means one unit cell of electric and magnetic potentials, not the primitive cell of carbon atoms.

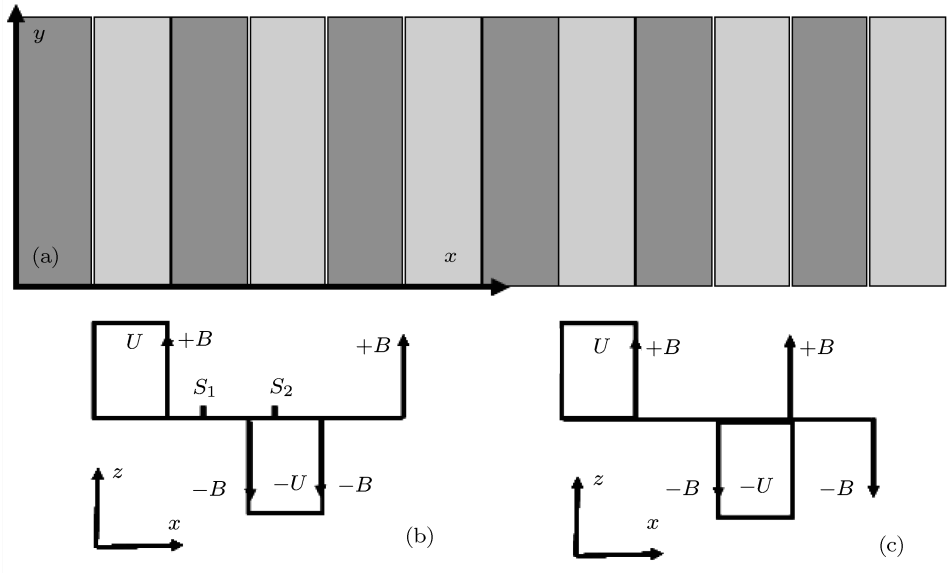


Fig. 1. (a) Schematic diagram of combined 1D electric and magnetic fields, which are arranged so that they are constant in the y direction and periodic in the x direction. We consider that the electric and magnetic fields are on average both zero in our calculation. (b) and (c) Two different unit cells (UCs) in which the electric and the magnetic potentials are arranged into different spatial symmetries.

Figures 2(a) and 2(b) show the lowest electron energy bands at different magnetic field strengths with $U = 3.0$ and 9.0, respectively. Here $w = b = 0.5$.

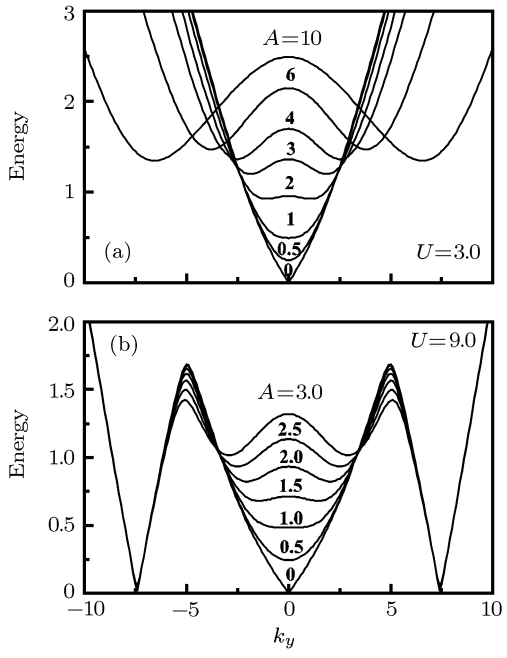


Fig. 2. The lowest electron energy band of single-layer graphene with model 1, in which $w = b = 0.5$, (a), $U = 3.0$, and $A = 0$, 0.5, 1.0, 2.0, 3.0, 4.0, 6.0, respectively; (b), $U = 9.0$, and $A = 0$, 0.5, 1.0, 1.5, 2.0, 2.5, 3.0, respectively.

It is seen that the shape of band changes gradually from triangle to flat band as the magnetic strength A increases from 0 to 3.0. As the magnetic field increases to over a threshold of ~ 1.5, the single energy valley splits into two valleys and the band bottom positions shift symmetrically away from $k_y = 0$ to $k_y \neq 0$ as shown in Figs. 3(a) and 3(b). The bandgap width increases gradually with magnetic field strength increasing, but finally saturates when the magnetic field strength is beyond 5.0.

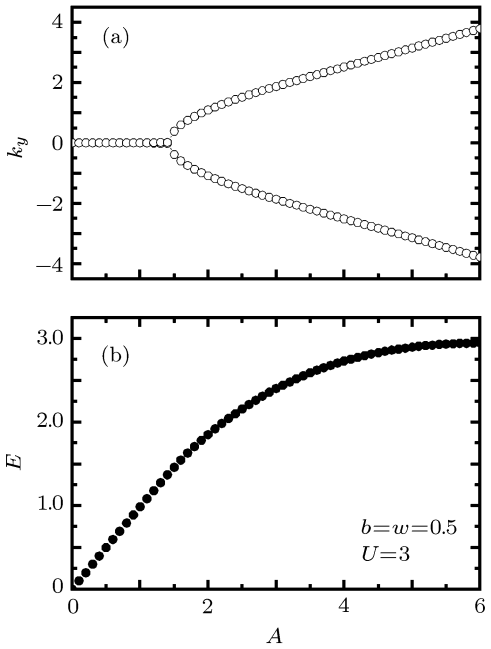


Fig. 3. (a) Band top/bottom positions as a function of the magnetic field strength; (b) the bandgap width as a function of the magnetic field strength, with model 1, where $w = b = 0.5$ and $U = 3.0$.

Secondly, we investigate the structures with a space barrier inserted into the unit cell (UC) of model 1 as shown in the inserts of Fig. 4. With inserting a space layer, equation (14) is no longer satisfied, the electron-hole symmetry is broken, and the single-layer graphene becomes an indirect bandgap semiconductor. It is easy to find that these four types of structures are related to each other by

$$(SP)H_{2a}(SP)^{-1} = -H_{2d}, \tag{15a}$$

$$(SP)H_{2b}(SP)^{-1} = -H_{2c}, \tag{15a}$$

$$SH_{2a}S^{-1} = H'_{2b}, \tag{15b}$$

$$SH_{2c}S^{-1} = H'_{2d}. \tag{15c}$$

From the above formulation, we can derive the relationships among those four band structures as follows: $E_{2a}(s,k_y) = E_{2b}(s,-k_y)$ and $E_{2c}(s,k_y) = E_{2d}(s,-k_y)$; $E_{2a}(s,k_y) = -E_{2d}(-s,k_y)$ and $E_{2b}(s,k_y) = -E_{2d}(-s,k_y)$.

Figures 4(a)–4(d) show the curves for electron energy E versus wave vector k_y for four types of single layers with the space layer in four different configurations. Here $w = w = b = 0.5$, $U = A = 3.0$ are taken in numerical calculations.

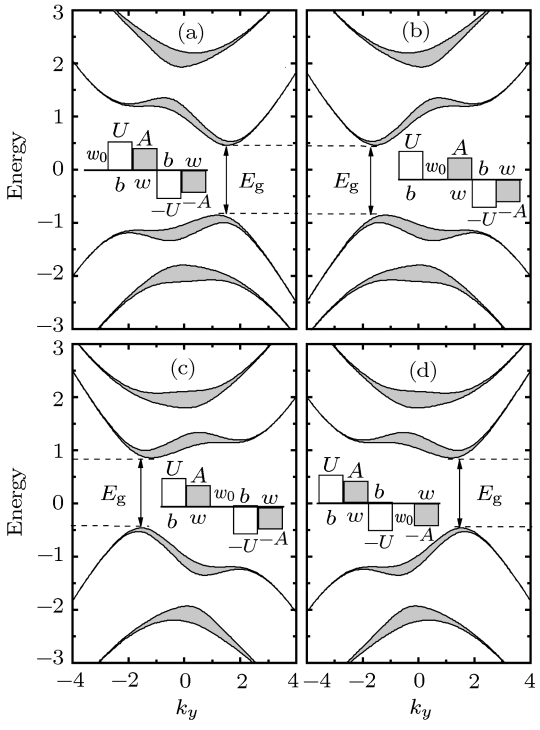


Fig. 4. Band structures of single-layer graphene, when a space layer is introduced into model 1 by four different configurations. The modified UC is shown by the insets in Figs. 4(a)–4(d). Here, $w = w = b = 0.5$ and $U = A = 3.0$.

It is seen that figure 4(a) becomes Fig. 4(d), and figure 4(b) becomes Fig. 4(c) by exchanging the electron and hole energy bands; figure 4(a) becomes Fig. 4(b) and figure 4(c) becomes Fig. 4(d) by exchanging k_y to $-k_y$. Obviously, single-layer graphenes in these types of structures are indirect bandgap semiconductors, while the widths of the bandgaps are the same for all four structures

Figure 5(a) and 5(b) illustrate the band top/bottom positions and the bandgap width as a function of space layer width w in the above four structures respectively. The bandgap width increases and both the band top/bottom positions shift away from $k_y = 0$ as w decreases. When $w = 0$, the band top and bottom appear at the same k_y position, and the single-layer graphene becomes a direct bandgap semiconductor and the maximum band opening is obtained.

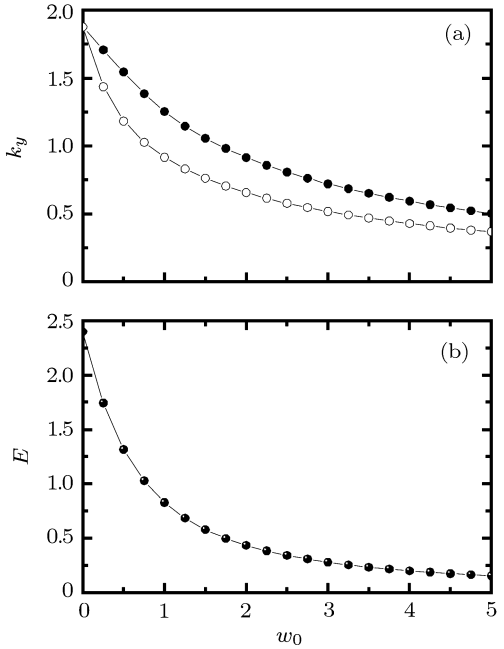


Fig. 5. Band top/bottom positions (a), and the bandgap width (b) as a function of w with models 2(a)–2(d), where $w = b = 0.5$ and $U = A = 3.0$.

Figures 6(a) and 6(b) show the electron band bottom position and the bandgap width as a function of the electric field strength U with $w_0 = 0$, respectively, where $A = 3.0$, and $b = w = 0.5$. As the electric field strength is less than 0.55π, a bandgap appears at $k_y = 0$, when the electric field strength is beyond 0.55π, the electron band splits into two energy valleys, and the band bottom positions shift away from $k_y = 0$ to $k_y \neq 0$, which is similar to what is shown in Fig. 3(a). However, the bandgap increases to a maximum at 0.9π, then decreases as the electric field strength increases, the bandgap closes at $k_y = 0$ when the electric field strength is equal to $n \cdot 2\pi$ since the

energy bandgap at $k_y = 0$ is a periodic function of electric field strength with a periodicity of π/b,[33−35,38] and the periodicity is not influenced by the magnetic field strength and its width as shown in Figs. 6(a) and 6(b).

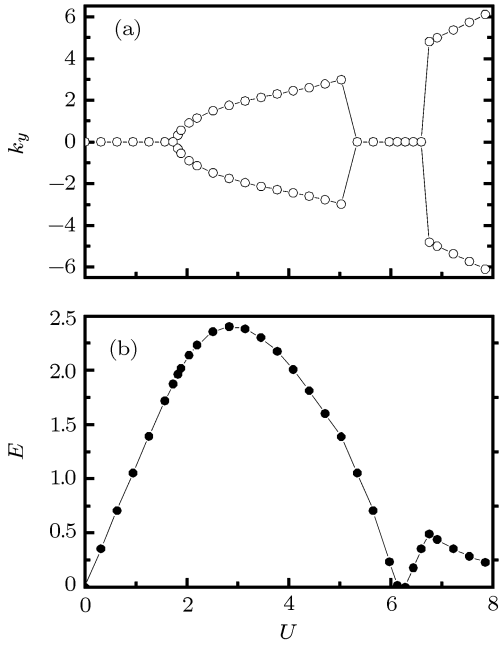


Fig. 6. Band top/bottom positions (a), and the bandgap width (b) as a function of U with model 1, where $w = b = 0.5$, and $A = 3.0$.

To confirm the gap opening in single-layer graphene, we calculate the transport property of single-layer graphene with finite periods of UC discussed in Section 3. The conductance G is obtained by using the Landauer–Buttiker formula

$$G(E_f) = \frac{4e^2}{h}\int_{-E_f}^{E_f} T(E_f, k_y)\frac{\mathrm{d}k_y}{2\pi/L_y} = G_0\int_{\pi/2}^{\pi/2} T(E_f, E_f\sin\theta)\cos\theta \mathrm{d}\theta, \quad (16)$$

where L_y is the sample size along the y direction, θ is the incident angle relative to the x direction, and $G_0 = 2e^2E_fL_y/\pi h$ is taken as the unit of conductance.

Figure 7 shows the curves for conductance (G/G_0) as a function of the energy E when electrons pass through the three UCs of model 1 and model 2(a). Here, we consider three different cases: electric barriers (EB) $U = 3.0$, $A = 0$; magnetic barriers (MB) $U = 0$, $A = 3.0$; and combined electric and magnetic barriers (EB+MB) $U = A = 3.0$. It can clearly be seen that the conductance always has a high value around $E = 0$ for EB due to Klein tunneling.

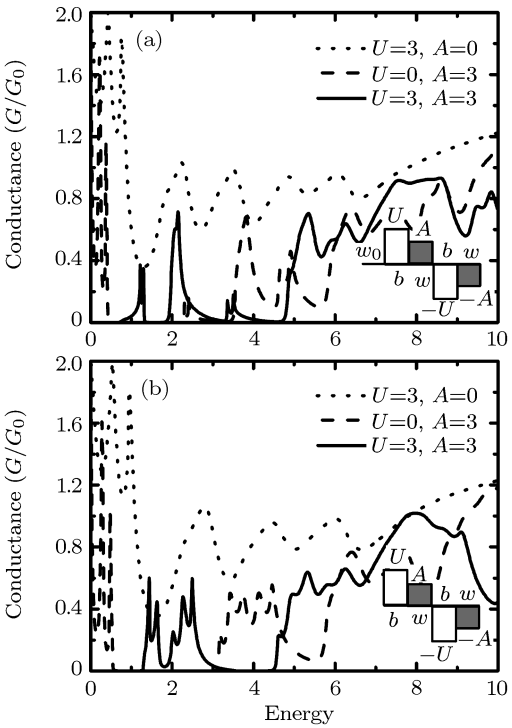


Fig. 7. Conductance (G/G_0) values as a function of the energy E, with three numbers of UC for model 1(a) and models 2(a) and 2(b). Here, $w = w = b = 0.5$ and $(U = 3.0,\ A = 0)$, $(U = 0,\ A = 3.0)$, $(U = A = 3.0)$ for three different cases.

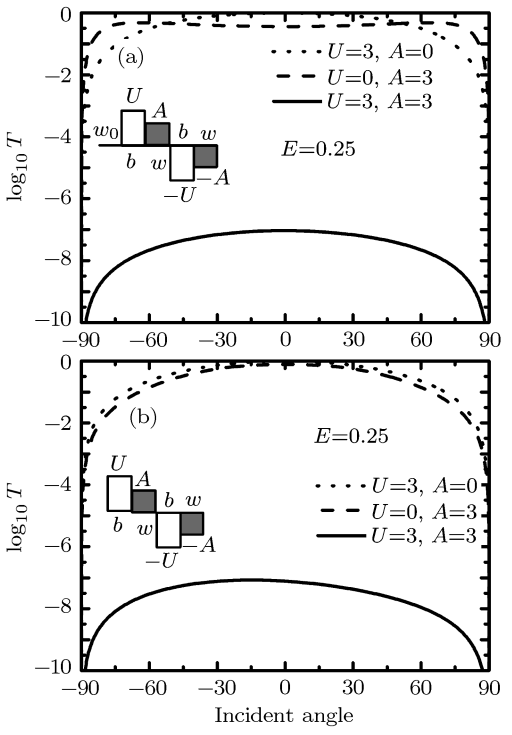


Fig. 8. Transmission possibilities as a function of the incident angle, with three numbers of UC for model 1(a) and models 2(a) and 2(b), when the electron energy $E = 0.25$ at the low energy area. Here, $w_0 = w = b = 0.5$ and $(U = 3.0,\ A = 0)$, $(U = 0,\ A = 3.0)$, $(U = A = 3.0)$ for three different cases.

For MB, the conductance around $E = 0$ has a

certain relatively high value, because the zero-energy model always holds in MB. While for the EB+MB case, the conductance is close to 0 in the low energy region, which demonstrates that the bandgap is generated at the Dirac point of the single-layer graphene. Figure 8 shows clearly that the transmission possibility of low energy electrons is almost 0 at any incident angle for the case EB+MB. Due to the gap opening, the zero-energy model will not hold in these kinds of structures, and the Klein tunneling is suppressed, which is completely different from the pristine graphene.

4. Conclusions

We have confirmed that a bandgap can be generated at the Dirac point in single-layer graphene under the modulation of combined 1D electric and magnetic fields. The bandgap, which acts as a mass term of Dirac fermions, originates from the coupling between electric and magnetic fields, which lift the two-fold degeneracy at the Dirac point. Therefore, single-layer graphene can be a direct or an indirect bandgap semiconductor, depending on the spatial configuration of the electric and magnetic fields. The bandgap width at the Dirac point varies periodically with the strength of the electric field increasing, and it increases monotonically with the strength of magnetic field increasing. Due to the bandgap generated in single-layer graphene, the zero-energy model is forbidden and the Klein tunneling observed in pristine graphene is completely suppressed.

As pointed out, the gap opening is of significant importance in design and fabrication of graphene-based electronics devices. Without cutting or etching, the combined electric and magnetic fields are easy to realize and control, which has wide applications in current semiconductor technology. Furthermore, the bandgap can be manipulated continuously by tuning the electric or magnetic field strength and their spatial configuration. The bandgap is estimated at ~ 40 meV for a UC length of 100 nm, $B \sim 0.8$ T and $U \sim 40$ meV, which is sufficient for electronic applications at room temperature. We hope that this striking feature can be explored experimentally in the future.

Appendix

Below, we evaluate the terms of the first part of Eq. (3). First, we take H_{11} for example.

$$H_{11} = \sum_{s,k} \frac{\langle \psi_1 | H' | \psi^0_{s,k} \rangle \langle \psi^0_{s,k} | H' | \psi_1 \rangle}{0 - E}, \tag{A1}$$

the summation $\sum_{s,k}$ means that H_{11} should be summed up over the whole band $s = \pm 1$ (both up band and down band). For convenience, we divide the whole band into eight symmetric parts as follows:

$$E > 0, \quad k_x > 0, \quad k_y > 0:$$

$$\psi^0_1 = \frac{1}{\sqrt{L}} . \frac{1}{\sqrt{2}} \begin{pmatrix} 1 \\ \mathrm{e}^{\mathrm{i}\,\theta_k} \end{pmatrix} \mathrm{e}^{\mathrm{i}\,k_x x} \mathrm{e}^{\mathrm{i}\,k_y y}; \tag{A2a}$$

$$E > 0, \quad k_x < 0, \quad k_y > 0:$$

$$\psi^0_2 = \frac{1}{\sqrt{L}} . \frac{1}{\sqrt{2}} \begin{pmatrix} 1 \\ -\mathrm{e}^{-\mathrm{i}\,\theta_k} \end{pmatrix} \mathrm{e}^{-\mathrm{i}\,k_x x} \mathrm{e}^{\mathrm{i}\,k_y y}; \tag{A2b}$$

$$E > 0, \quad k_x > 0, \quad k_y < 0:$$

$$\psi^0_3 = \frac{1}{\sqrt{L}} . \frac{1}{\sqrt{2}} \begin{pmatrix} 1 \\ \mathrm{e}^{\mathrm{i}\,\theta_k} \end{pmatrix} \mathrm{e}^{\mathrm{i}\,k_x x} \mathrm{e}^{-\mathrm{i}\,k_y y}; \tag{A2c}$$

$$E > 0, \quad k_x < 0, \quad k_y < 0:$$

$$\psi^0_4 = \frac{1}{\sqrt{L}} . \frac{1}{\sqrt{2}} \begin{pmatrix} 1 \\ -\mathrm{e}^{\mathrm{i}\,\theta_k} \end{pmatrix} \mathrm{e}^{-\mathrm{i}\,k_x x} \mathrm{e}^{-\mathrm{i}\,k_y y}; \tag{A2d}$$

$$E < 0, \quad k_x > 0, \quad k_y > 0:$$

$$\psi^0_5 = \frac{1}{\sqrt{L}} . \frac{1}{\sqrt{2}} \begin{pmatrix} 1 \\ -\mathrm{e}^{\mathrm{i}\,\theta_k} \end{pmatrix} \mathrm{e}^{\mathrm{i}\,k_x x} \mathrm{e}^{\mathrm{i}\,k_y y}; \tag{A2e}$$

$$E < 0, \quad k_x < 0, \quad k_y > 0:$$

$$\psi^0_6 = \frac{1}{\sqrt{L}} . \frac{1}{\sqrt{2}} \begin{pmatrix} 1 \\ \mathrm{e}^{-\mathrm{i}\,\theta_k} \end{pmatrix} \mathrm{e}^{-\mathrm{i}\,k_x x} \mathrm{e}^{\mathrm{i}\,k_y y}; \tag{A2f}$$

$$E < 0, \quad k_x > 0, \quad k_y < 0:$$

$$\psi^0_7 = \frac{1}{\sqrt{L}} . \frac{1}{\sqrt{2}} \begin{pmatrix} 1 \\ -\mathrm{e}^{-\mathrm{i}\,\theta_k} \end{pmatrix} \mathrm{e}^{\mathrm{i}\,k_x x} \mathrm{e}^{-\mathrm{i}\,k_y y}; \tag{A2g}$$

$$E < 0, \quad k_x < 0, \quad k_y < 0:$$

$$\psi^0_8 = \frac{1}{\sqrt{L}} . \frac{1}{\sqrt{2}} \begin{pmatrix} 1 \\ \mathrm{e}^{\mathrm{i}\,\theta_k} \end{pmatrix} \mathrm{e}^{-\mathrm{i}\,k_x x} \mathrm{e}^{-\mathrm{i}\,k_y y}. \tag{A2h}$$

Where $1/\sqrt{L}$ is a box normalization factor, and θ_k is the polar angle of the wave vector $\boldsymbol{k} = (|k_x|, |k_y|)$. Now, H_{11} can be further expressed as

$$H_{11} = \sum_{s=1, k_x>0, k_y>0} \sum_{i=1,8} S_i, \tag{A3}$$

$$S_i = \frac{\langle \psi^0_i | H' | \psi^0_{s,k} \rangle \langle \psi^0_{s,k} | H' | \psi^0_i \rangle}{0 - E}. \tag{A4}$$

Sum up $\sum_{i=1,8} S_i$, then we will have

$$H_{11} = \sum_{s=1,k_x>0,k_y>0} I_{11}, \tag{A5}$$

$$\begin{aligned} I_{11} =& \frac{1}{L^2}\frac{1}{E} 8 v_{\mathrm{F}} \cos\theta_k \Bigg(\int_0^L \mathrm{d}x e U(x) \sin(k_x x) \\ & \times \int_0^L \mathrm{d}x e A(x) \cos(k_x x) \\ & - \int_0^L \mathrm{d}x e U(x) \cos(k_x x) \\ & \times \int_0^L \mathrm{d}x e A(x) \sin(k_x x) \Bigg), \end{aligned} \tag{A6}$$

with

$$k_x = k\cos\theta_k, \quad k_x = k\sin\theta_k, \quad k = E/v_{\mathrm{F}}.$$

Convert the sum $\sum_{s=1,k_x>0,k_y>0}$ into integer, i.e.,

$$H_{11} = \int_{s=1,k_x>0,k_y>0} \mathrm{d}E k \mathrm{d}\theta_k \rho(E,\theta_k) I_{11}, \tag{A7}$$

where

$$\rho(E,\theta_k) = \frac{2A_{\mathrm{c}}E}{\pi \cdot v_{\mathrm{F}}^2} \frac{1}{2\pi k} = \frac{A_{\mathrm{c}}}{\pi^2 v_{\mathrm{F}}} \tag{A8}$$

with A_{c} being a unit cell area of graphene honeycomb lattice.

By the same steps, we can also obtain

$$H_{22} = -H_{11}, \qquad H_{12} = H_{21} = 0.$$

References

[1] Novoselov K S, Geim A K, Morozov S V, Jiang D, Zhang Y, Dubonos S V, Grigorieva I V and Firsov A A 2004 *Science* **306** 666

[2] Bolotin K, Sikes K, Jiang Z, Klima M, Fudenberg G, Hone J, Kim P and Stormer H L 2008 *Solid State Commun.* **146** 351

[3] Neugebauer P, Orlita M, Faugeras C, Barra A L and Potemski M 2009 *Phys. Rev. Lett.* **103** 136403

[4] Neto H C, Guinea F, Peres N M R, Novoselov K S and Geim A K 2009 *Rev. Mod. Phys.* **81** 109

[5] Beenakker W J 2008 *Rev. Mod. Phys.* **80** 1337

[6] Novoselov K S, Geim A K, Morozov S V, Jiang D, Katsnelson M I, Grigorieva I V, Dubonos S V and Firsov A A 2005 *Nature* **438** 197

[7] Zhang Y, Tan J W, Stormer H L and Kim P 2005 *Nature* **438** 201

[8] Zhou S Y, Gweon G H, Fedorov A V, First P N, Deheer W A, Lee D H, Guinea F, Castro Neto A H and Lanzara1 A 2007 *Nat. Mater.* **6** 770

[9] Gusynin V P and Sharapov S G 2005 *Phys. Rev. Lett.* **95** 146801

[10] Katsnelson M I, Novoselov K S and Geim A K 2006 *Nat. Phys.* **2** 620

[11] Novoselov K S, Jiang D, Booth T, Khotkevich V V, Morozov S M and Geim A K 2005 *Proc. Natl. Acad. Sci. USA* **102** 10451

[12] Guinea F, Katsnelson M I and Geim A K 2010 *Nat. Phys.* **6** 30

[13] Balog R, Jørgensen B, Nilsson1 L, Andersen M, Rienks E, Bianchi M, Fanetti M, Lægsgaard E, Baraldi A, Lizzit S, Sljivancanin Z, Besenbacher F, Hammer B, Pedersen T G, Hofmann P and Hornekær L 2010 *Nat. Mater.* **9** 315

[14] Meyer J C, Girit C O, Crommie M F and Zettl A 2008 *Appl. Phys. Lett.* **92** 123110

[15] Yang J, Dong Q L, Jiang Z T and Zhang J 2010 *Chin. Phys.* B **19** 127104

[16] Han M Y, Ozyilmaz B, Zhang Y and Kim P 2007 *Phys. Rev. Lett.* **98** 206805

[17] Zhang L J and Xia T S 2010 *Chin. Phys.* B **19** 117105

[18] Son Y W, Cohen M L and Louie S G 2006 *Phys. Rev. Lett.* **97** 216803

[19] Pedersen T G, Flindt C, Pedersen J, Mortensen N A, Jauho A P and Pedersen K 2008 *Phys. Rev. Lett.* **100** 136804

[20] Rotenberg E, Bostwick A, Ohta T, McChesney J L, Seyller T and Horn K 2008 *Nat. Mater.* **7** 258

[21] Zhou S Y, Siegel D A, Fedorov A V, Gabaly F E, Schmid A K, Castro Neto A H, Lee D H and Lanzara1 A 2008 *Nat. Mater.* **7** 259

[22] Gerhardts R R, Weiss D and Klitzing K V 1989 *Phys. Rev. Lett.* **62** 1173

[23] Peeters F M and Matulis A 1993 *Phys. Rev.* B **48** 20

[24] Matulis A and Peeters F M 1994 *Phys. Rev. Lett.* **72** 1518

[25] Messica A, Soibel A, Meirav U, Stern A, Shtrikman H, Umansky V and Mahalu D 1997 *Phys. Rev. Lett.* **78** 705

[26] Kato M, Endo A, Katsumoto S and Iye Y 1998 *Phys. Rev.* B **58** 4876

[27] Zhai F and Chang K 2008 *Phys. Rev.* B **77** 113409

[28] Masir M R, Vasiopoulos P and Peeters F M 2009 *Phys. Rev.* B **79** 035409

[29] Huard B, Sulpizio J A, Stander N, Todd K, Yang B and Goldhaber-Gordon D 2007 *Phys. Rev. Lett.* **98** 236803

[30] Williams J R, Carlo L Di and Marcus C M 2007 *Science* **317** 638

[31] Haugen H, Huertas-Hernando D and Brataas A 2008 *Phys. Rev.* B **77** 115406

[32] Lin X, Pan H and Xu H Z 2010 *Commun. Theor. Phys.* **54** 1134

[33] Park C H, Yang L, Son Y W, Cohen M L and Louie S G 2008 *Nat. Phys.* **4** 213

[34] Park C H, Yang L, Son Y W, Cohen M L and Louie S G 2008 *Phys. Rev. Lett.* **101** 126804

[35] Park C H, Son Y W, Yang L, Cohen M L and Louie S G 2008 *Nano Lett.* **8** 2920

[36] Brey L and Fertig H A 2009 *Phys. Rev. Lett.* **103** 046809

[37] Barbier M, Vasiopoulos P and Peeters F M 2010 *Phli. Trans. R. Soc.* A **368** 5499

[38] Park C H, Son Y W, Yang L, Cohen M L and Louie S G 2009 *Phys. Rev. Lett.* **103** 046808

[39] Barbier M, Vasiopoulos P and Peeters F M 2009 *Phys. Rev.* B **80** 205415

[40] Barbier M, Peeters F M, Vasiopoulos P and Pereira J M 2008 *Phys. Rev.* B **77** 115446

[41] Wang L G and Zhu S Y 2010 *Phys. Rev.* B **81** 205444

[42] Park C H, Tan L Z and Louie S G 2011 *Physica* E **43** 651

[43] Masir M R, Vasiopoulos P and Peeters F M 2009 *New J. Phys.* **11** 095009

[44] Masir M R, Vasiopoulos P, Matulis A and Peeters F M 2008 *Phys. Rev.* B **77** 235443

[45] DeMartino A, Dell'Anna L and Egger R 2007 *Phys. Rev. Lett.* **98** 066802

[46] DeMartino A, Dell'Anna L and Egger R 2009 *Phys. Rev.* B **79** 045420

[47] Xu L, An J and Gong C D 2010 *Phys. Rev.* B **81** 125424

[48] Tan L Z, Park C H and Louie S G 2010 *Phys. Rev.* B **81** 195426

[49] Snyman I 2009 *Phys. Rev.* B **80** 054303

[50] Barbier M, Vasiopoulos P and Peeters F M 2010 *J. Phys.: Condens. Matter* **22** 465302

[51] Meyer J C, Girit C O, Crommie M F and Zettl A 2008 *Appl. Phys. Lett.* **92** 123110